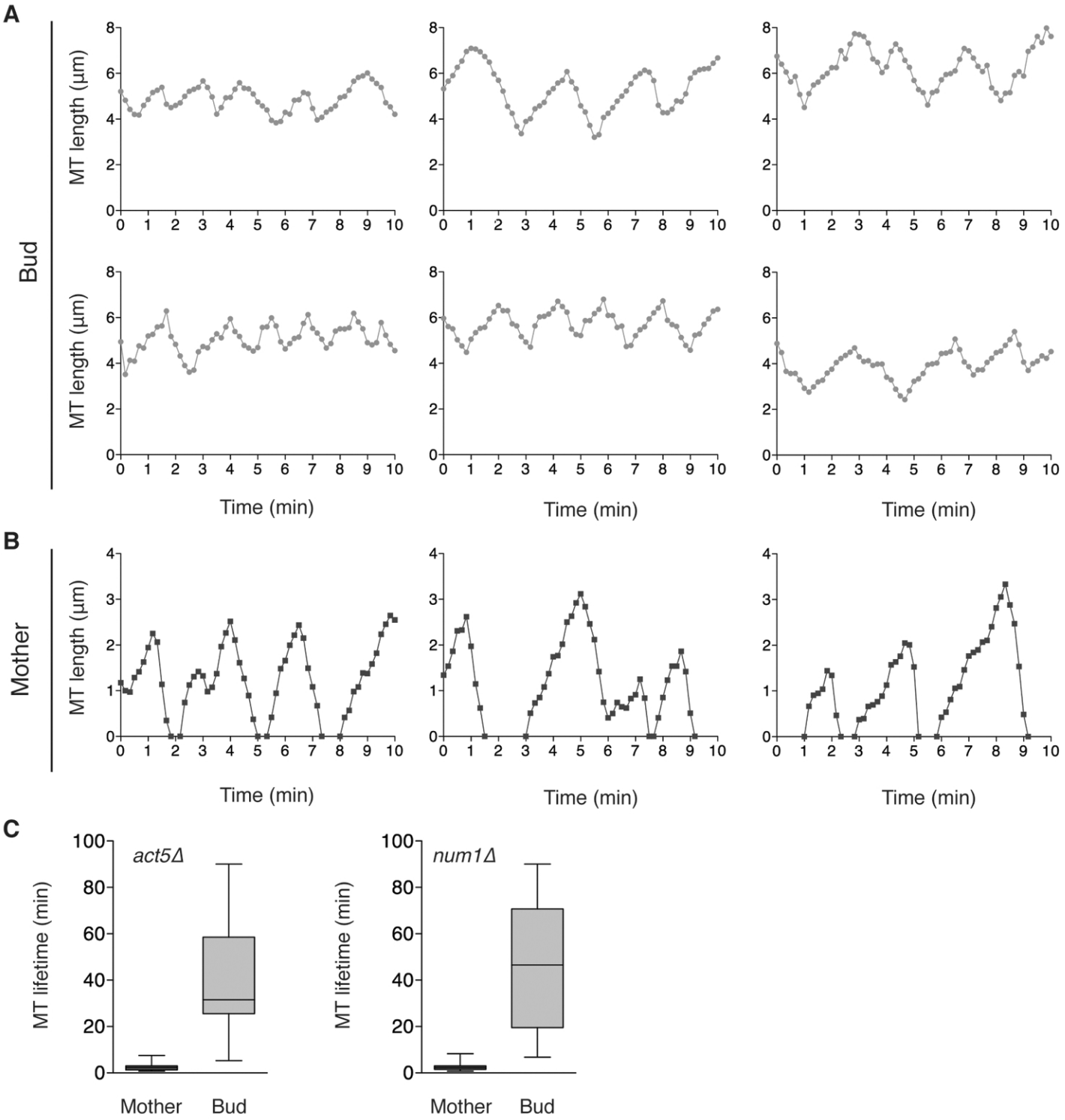

Figure S1. Microtubule lifetime is differentially regulated within cells with mispositioned spindles. Related to Figure 1. (A and B) Additional examples of lifetime history plots for astral microtubules (MTs) in the (A) bud or (B) mother compartment of *dyn1Δ* cells with mispositioned spindles. Each graph represents a separate cell. In (A) the spindle pole is varying distances from the bud neck, and no MT depolymerizes past the bud neck, in each cell. (C) A boxplot of astral MT lifetimes within the mother and bud of *act5Δ* or *num1Δ* cells with mispositioned spindles. For mother MTs n = 46 and 46, for bud MTs n = 19 and 20 for *act5Δ* and *num1Δ* cells, respectively. For both cell types, $P < 0.0001$ for mother vs. bud MT lifetimes. The center line represents the median, the boxes encompass the 25th to 75th percentiles, and the bars extend from the minimum to the maximum values.

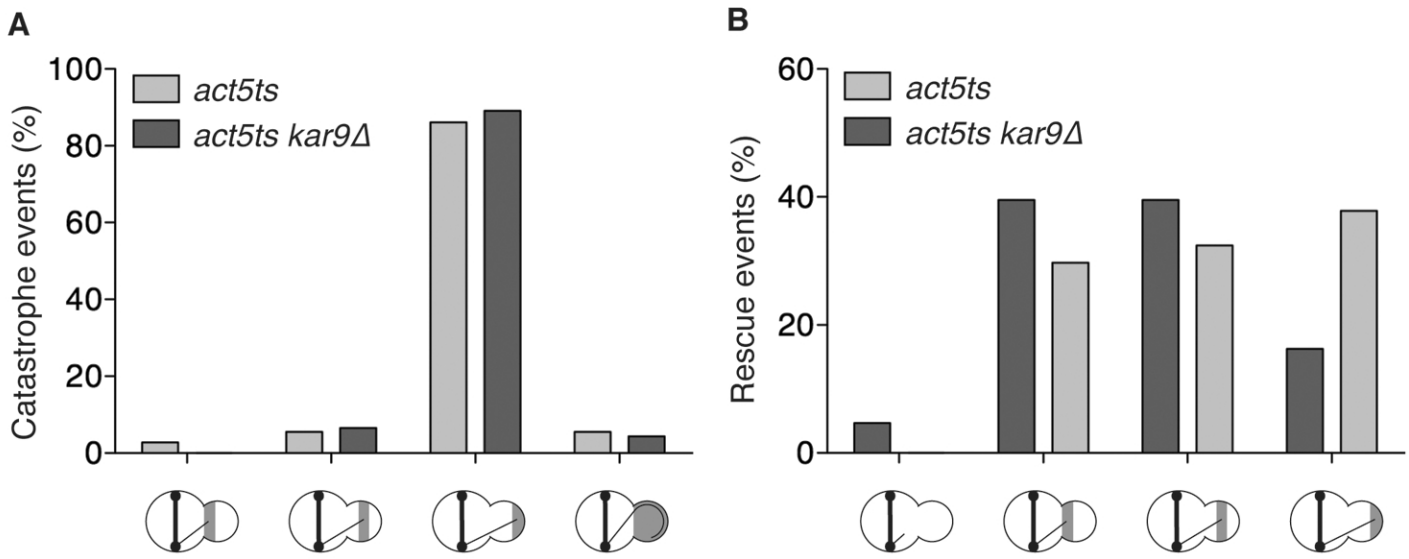

Figure S2. Spatial regulation of microtubule catastrophe and rescue is independent of Kar9. Related to Figure 2. Location of microtubule (MT) catastrophe (A) and rescue (B) events in the bud of *act5ts* and *act5ts kar9Δ* cells at restrictive temperature (37°C, 1 h 45 min). For catastrophe and rescue n = 36 and 37, and n = 46 and 43 for *act5ts* and *act5ts kar9Δ* cells, respectively. The X-axis demarks events that occur within each third of the bud. In (A), the far right category represents MTs that overgrow the bud and curl around the bud tip prior to catastrophe. In (B), the far left category represents MTs that depolymerize out of the bud without undergoing rescue.

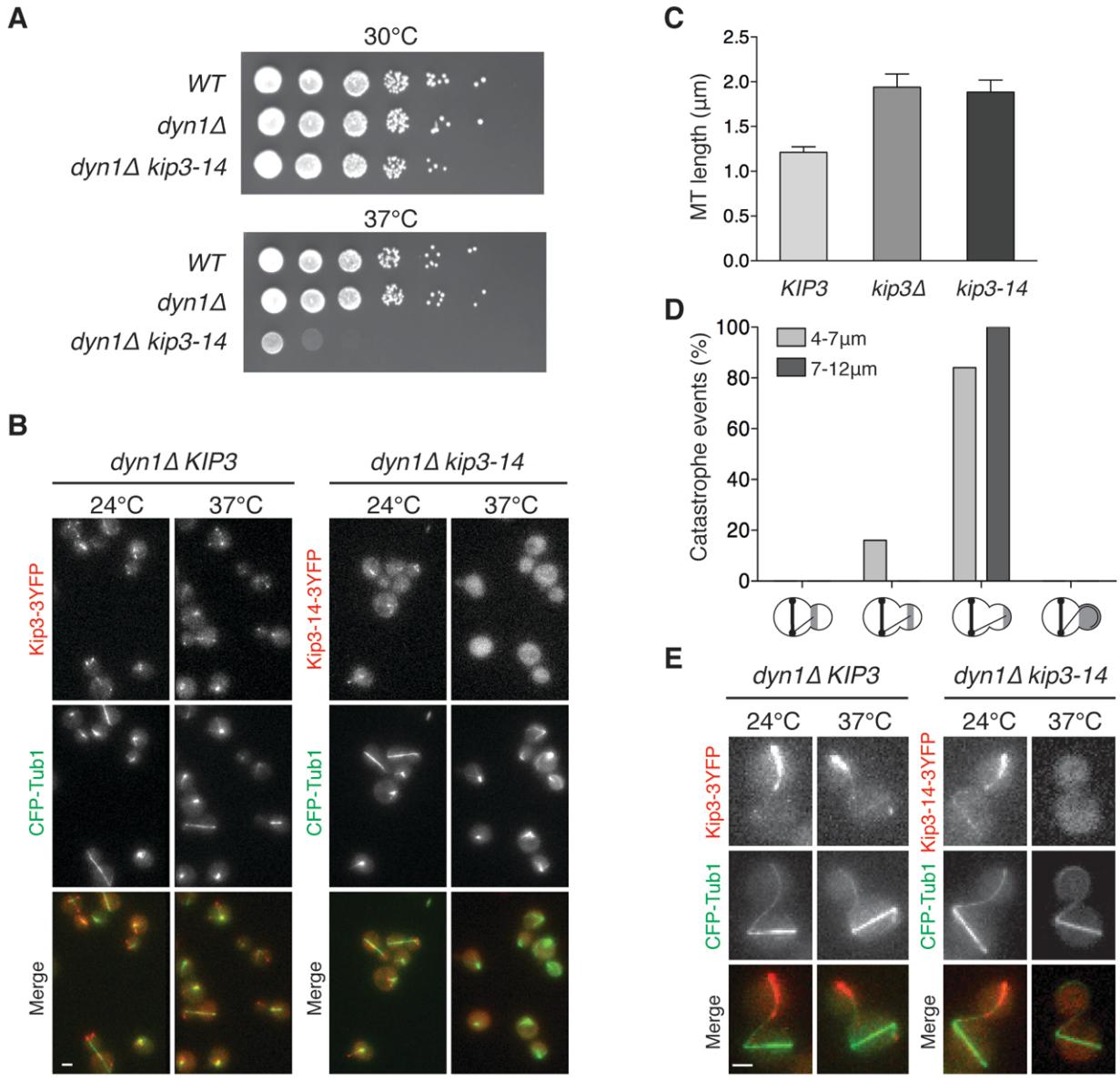

Figure S3. Inactivation of the *kip3-14* allele leads to loss of Kip3 function. Related to Figure 3. (A) Inactivation of *kip3-14* results in synthetic lethality with *dyn1Δ*. Indicated strains are spotted in 10-fold serial dilutions and incubated at 30°C and 37°C. (B) Localization of Kip3-14 is lost at restrictive temperature at all stages of the cell cycle. Representative images depicting localization of Kip3 and Kip3-14. Kip3-3YFP is properly localized in *dyn1Δ* cells at both permissive (24°C) and restrictive temperature (37°C). Kip3-14-3YFP is properly localized in *dyn1Δ kip3-14* cells at 24°C, but is no longer found on microtubules (MTs) after 1 hr at restrictive temperature. Scale bar represents 2μm. (C) MT length during G1 in *KIP3*, *kip3Δ* and *kip3-14* cells. Mean ± SEM, n > 80, P < 0.0001 for *KIP3* vs *kip3Δ* and *KIP3* vs *kip3-14*. (D) Location of catastrophe events within the bud of *dyn1Δ KIP3* cells according to MT length. MTs are categorized as short (4-7μm) or long (7-12μm) based on the length at catastrophe. The X-axis demarks events that occur within each third of the bud. The far right category represents MTs that overgrow the bud and curl around the bud tip prior to catastrophe. n = 50 and 42 for MTs ranging from 4-7μm and 7-12μm, respectively. (E) Localization of Kip3-14-3YFP along bud MTs is lost at restrictive temperature in cells with mispositioned spindles. Scale bar represents 2μm.

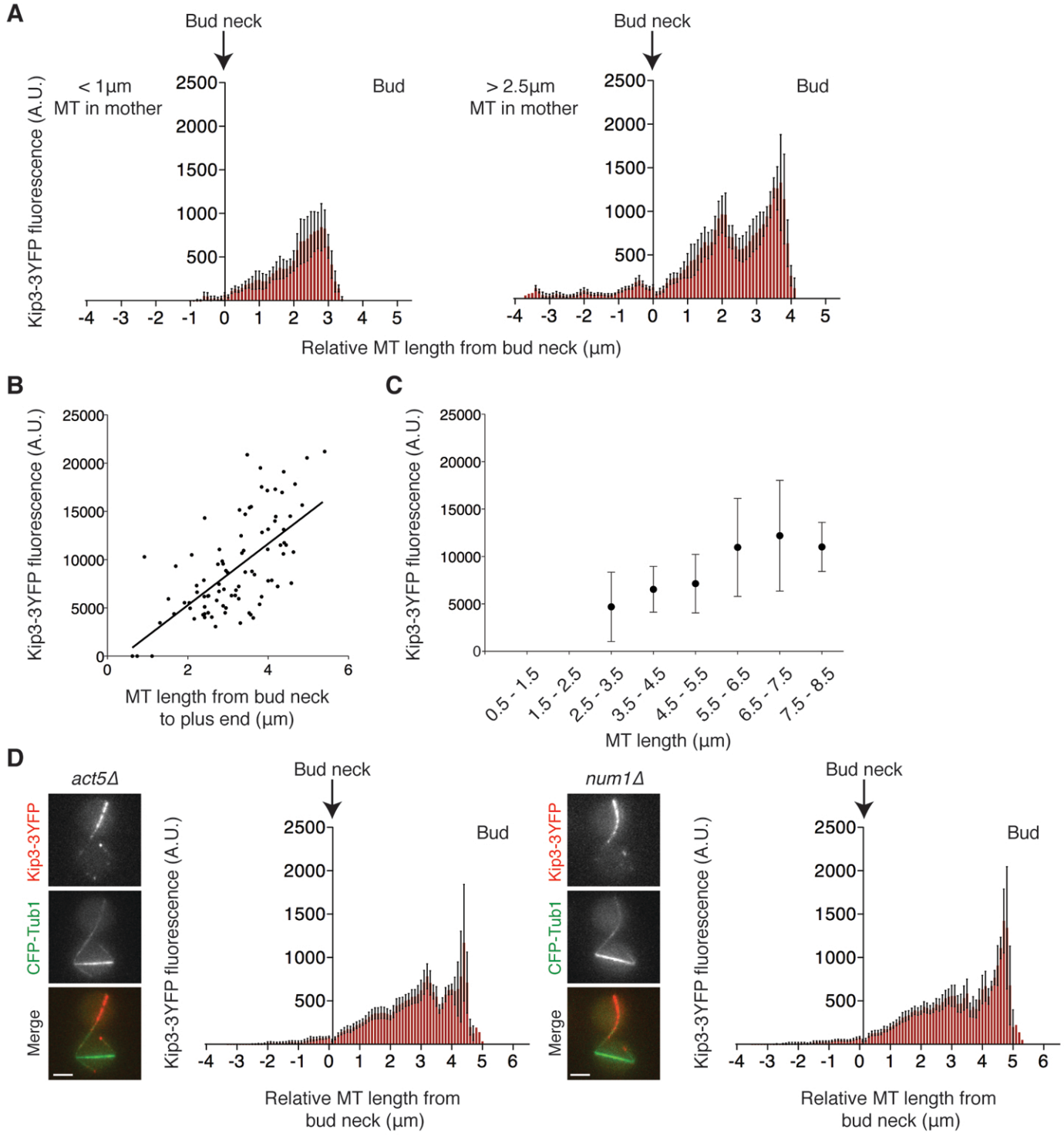

Figure S4. Kip3 accumulates along the length of microtubules in the bud of cells with mispositioned spindles. Related to Figure 4. (A) The average Kip3-3YFP fluorescence signal along bud microtubules (MTs) that have short (left) or long (right) MT segments in the mother compartment. The MTs are aligned so that 0µm represents where each MT crosses the bud neck. For MTs with short and long mother segments n = 5 and 6, respectively. (B) Scatter plot of data presented in Figure 4D. $P < 0.0001$, n = 94 plus-ends. (C) The MTs presented in Figure 4D are binned according to total length from spindle pole to plus-end, n = 94 plus-ends. (D) The average Kip3-3YFP fluorescence signal along bud MTs in *act5Δ* cells (left) and *num1Δ* cells (right) aligned so that 0µm represents where each MT crosses the bud neck. For *act5Δ* and *num1Δ* cells n = 16 and 16 MTs, respectively. The micrographs depict a representative cell. In (A) and (D) the fluorescence intensity scale is identical, the spindle pole is toward the left and the plus-end toward the right for each graph. Scale bars are 2µm.

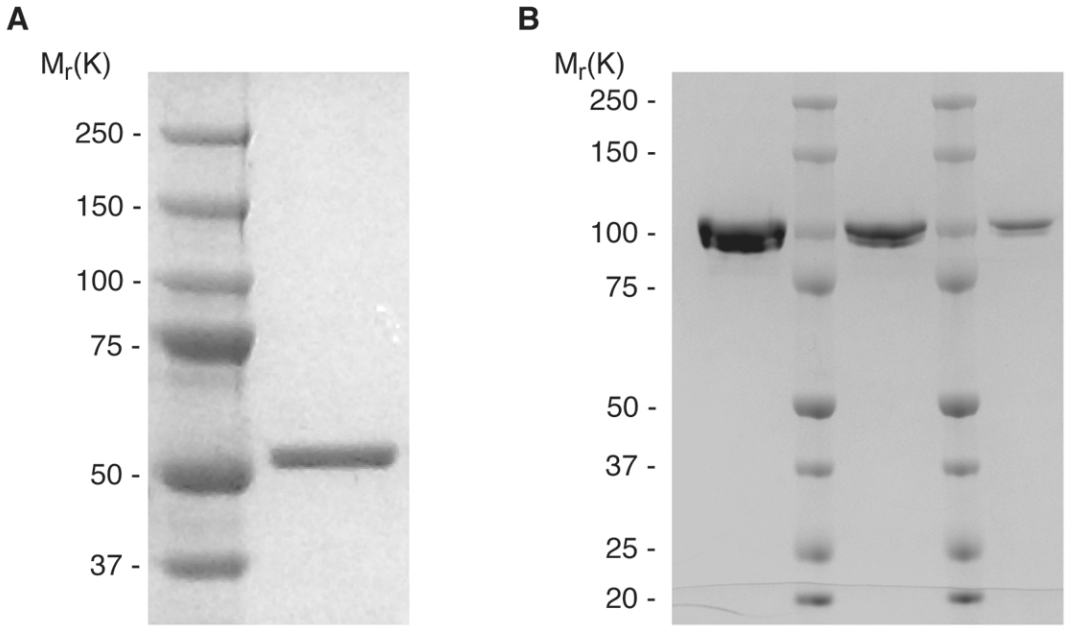

Figure S5. Purification of yeast tubulin and Kip3. Related to Figure 5. Coomassie-stained gels loaded with (A, from left) molecular weight standards (MW) and 3μg purified tubulin from yeast cells or (B, from left) 9.4μg purified Kip3, MW, 4.7μg purified Kip3, MW, and 1.9μg purified Kip3 produced in insect cells.

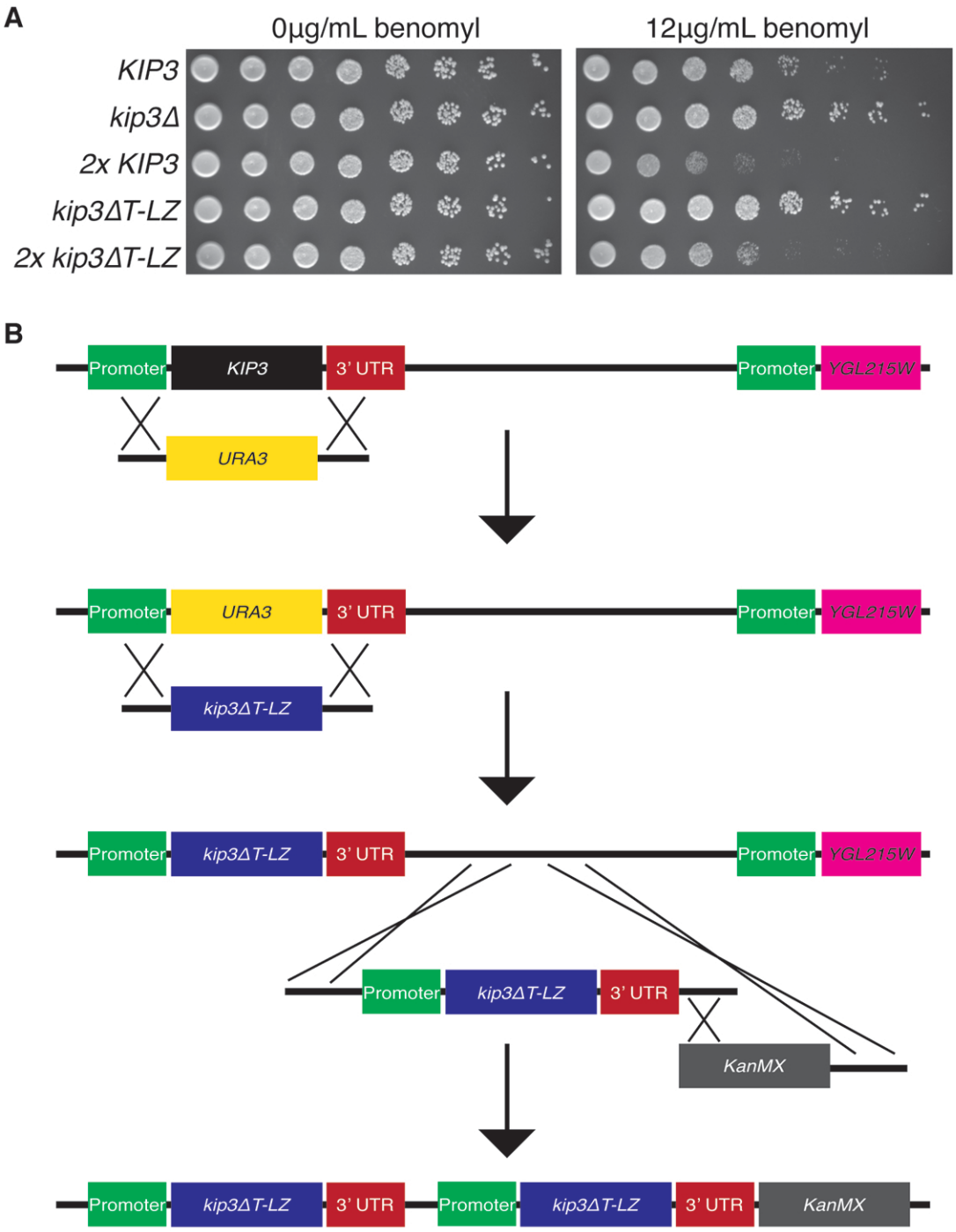

Figure S6. Wild-type levels of benomyl sensitivity require two copies of non-tagged *kip3ΔT-LZ*. Related to Figure 6. (A) Benomyl sensitivity of cells expressing various copy numbers of *KIP3* or *kip3ΔT-LZ* each under their own regulatory elements. From the left, 10-fold serial dilutions of cells are plated on rich media alone, or containing 12µg/mL benomyl. (B) Strategy for introducing one or two copies of non-tagged *kip3ΔT-LZ* in place of endogenous *KIP3*. Please refer to Supplemental Experimental Procedures for a detailed description of the methods.

Table S1. Dynamic instability of astral microtubules *in vivo*.

***dyn1Δ KIP3*, 24°C**	**Bud microtubules**	**Mother microtubules**
Growth rate (μm min^{-1})	1.58 ± 0.37 (65)	1.47 ± 0.43 (80)
Depolymerization rate (μm min^{-1})	2.30 ± 0.60 (64)*	2.99 ± 0.87 (80)*
Catastrophe frequency (min^{-1})	0.73 (60)	0.73 (71)
neck-proximal third of bud	0.00 (0)	n.a.
central third of bud	0.23 (9)	n.a.
tip-proximal third of bud	1.40 (87)	n.a.
Rescue frequency (min^{-1})	0.91 (54)	0.47 (25)
neck-proximal third of bud	2.34 (30)	n.a.
central third of bud	1.17 (40)	n.a.
tip-proximal third of bud	0.54 (28)	n.a.
Time spent growing (%)	58.0	61.9
Time spent shortening (%)	42.0	35.5
Time spent attenuated (%)	0	2.7
***dyn1Δ KIP3*, 37°C**		
Growth rate (μm min^{-1})	2.45 ± 0.56 (43)	n.d.
Depolymerization rate (μm min^{-1})	3.66 ± 0.98 (47)**	n.d.
***dyn1Δ kip3-14*, 37°C**		
Growth rate (μm min^{-1})	2.48 ± 0.66 (31)	n.d.
Depolymerization rate (μm min^{-1})	6.43 ± 1.95 (41)**	n.d.

The mean parameters of dynamic instability are calculated from 150 and 142 min of total lifetime for MTs that remained within the mother and bud compartments, respectively, of 13 cells with spindles mispositioned within the mother cell. Localized catastrophe and rescue frequencies within the bud are determined from 99 and 119 min of total growth and shortening time, respectively, within the bud. For transition frequencies the variance is not determined because transitions did not occur stochastically, rather they were induced spatially within the bud (see Figure 2). MT growth and depolymerization rate within the bud of cells with mispositioned spindles in *dyn1Δ KIP3* and *dyn1Δ kip3-14* cells after 1hour at 37°C. All rates are reported as the mean ± SD. The number of events is in parentheses. *$P < 0.0001$ for depolymerization rates between mother and bud in *dyn1Δ KIP3* cells at 24°C. **$P < 0.0001$ for bud microtubule depolymerization rates between *dyn1Δ KIP3* and *dyn1Δ kip3-14* at 37°C.

Table S2. Yeast strains and plasmids used in this study. Related to Experimental Procedures.

Yeast Strain	Genotype	Source
MGY1551	MAT**a** *ura3-52 his3-Δ200 leu2-Δ1 trp1-Δ63*	S288C control
MGY1552	MAT**α** *ura3-52 his3-Δ200 leu2-Δ1 trp1-Δ63*	S288C control
MGY1553	MAT**a** *dyn1Δ::TRP1 ura3-52 his3-Δ200 leu2-Δ1*	This study
MGY1554	MAT**a** *dyn1Δ::TRP1 kip3Δ::kip3-14 ura3-52 his3-Δ200 leu2-Δ1*	This study
MGY1586	MAT**a** *dyn1Δ::TRP1 kip3Δ::kip3ΔT-LZ 2x kip3ΔT-LZ::KanMX ura3-52 his3-Δ200 leu2-Δ1*	This study
MGY1587	MAT**a** *kip3Δ::URA3 his3-Δ200 leu2-Δ1 trp1-Δ63*	This study
MGY1561	MAT**a** *kip3Δ::kip3ΔT-LZ ura3-52 his3-Δ200 leu2-Δ1 trp1-Δ63*	This study
MGY1562	MAT**a** *kip3Δ::kip3ΔT-LZ 2x kip3ΔT-LZ::KanMX ura3-52 his3-Δ200 leu2-Δ1 trp1-Δ63*	This study
MGY1563	MAT**a** *KIP3 2x KIP3::KanMX ura3-52 his3-Δ200 leu2-Δ1 trp1-Δ63*	This study
MGY1555	MAT**a** *dyn1Δ::TRP1 GFP-TUB1::LEU2 ura3-52 his3-Δ200*	This study
MGY1556	MAT**a** *dyn1Δ::TRP1 GFP-TUB1::LEU2 ura3-52 his3-Δ200*	This study
MGY1557	MAT**a** *dyn1Δ::TRP1 GFP-TUB1::LEU2 kip3Δ::kip3-14 ura3-52 his3-Δ200*	This study
MGY1572	MAT**a** *dyn1Δ::TRP1 GFP-TUB1::LEU2 kip3Δ::kip3ΔT-LZ 2x kip3ΔT-LZ::KanMX ura3-52 his3-Δ200*	This study
MGY1577	MAT**a** *dyn1Δ::TRP1 GFP-TUB1::LEU2 KIP3 2x KIP3::KanMX ura3-52 his3-Δ200*	This study
MGY1588	MAT**a** *GFP-Tub1::LEU2 ura3-52 his3-Δ200 trp1-Δ63*	This study
MGY1589	MAT**a** *GFP-Tub1::LEU2 kip3Δ::URA3 his3-Δ200 trp1-Δ63*	This study
MGY1590	MAT**a** *GFP-Tub1::LEU2 kip3Δ::kip3-14 ura3-52 his3-Δ200 trp1-Δ63*	This study
MGY1558	MAT**a** *dyn1Δ::HIS3 CFP-TUB1::URA3 KIP3-3YFP::LEU2 trp1-Δ63*	This study
MGY1559	MAT**a** *dyn1Δ::TRP1 CFP-TUB1::URA3 kip3-14-3YFP::LEU2 his3-Δ200*	This study
MGY1560	MAT**a** *CSE4-YFP::HIS5 ura3-52 leu2-Δ1 trp1-Δ63*	This study
MGY1579	MAT**a** *KIP3-EYFP::HIS5 CFP-TUB1::URA3 dyn1Δ::TRP1 leu2-Δ1*	This study
MGY1609	MAT**a** *kip3Δ::kip3ΔT-LZ-EYFP::KanMX 2x kip3ΔT-LZ::NatMX CFP-TUB1::URA3 dyn1Δ::TRP1 his3-Δ200 leu2-Δ1*	This study
MGY1681	MAT**a** *act5Δ::TRP1 GFP-TUB1::LEU2 ura3-52 his3-Δ200*	This study
MGY1646	MAT**a** *num1Δ::TRP1 GFP-TUB1::LEU2 ura3-52 his3-Δ200*	This study
MGY1716	MAT**a** *act5Δ::TRP1 CFP-TUB1::URA3 KIP3-3YFP::LEU2 his3-Δ200*	This study

Table S2 (cont.)

MGY1619	MAT**a** *num1∆::TRP1 CFP-TUB1::URA3 KIP3-3YFP::LEU2 his3-∆200*	This study
MGY1717	MAT**a** *cdc15-2::KanMX dyn1∆::TRP1 GFP-TUB1::LEU2 ura3-52 his3-∆200*	This study
MGY1639	MAT**a** *cdc15-2::KanMX dyn1∆::TRP1 bfa1∆::HIS3 GFP-TUB1::LEU2 ura3-52*	This study
MGY1718	MAT**a** *act5∆::TRP1 act5ts::LEU2 TUB1-GFP::URA3 his3-∆200*	This study
MGY1272	MAT**a** *act5∆::TRP1 act5ts::LEU2 TUB1-GFP::URA3 kar9∆::HIS3*	This study
MGY1591	MAT**a** *kip3Δ::KanMX kip3ΔT-LZ-EYFP::LEU2 CFP-TUB1::URA3 his3-∆200 trp1-∆63*	Su et al. [S1]

Plasmid	**Genotype**	**Source**
pFC51*kip3-14*	CEN *kip3-14 LYS2* AmpR	Cottingham and Hoyt [S2]
pBJ781	*act5ts LEU2* AmpR	Muhua et a. [S3]

Supplemental Experimental Procedures

Yeast strains

Yeast strains were derivatives of S288C background (Table S2). To generate *dyn1Δ kip3-14* cells expressing GFP-Tubulin, the *kip3-14* allele (which codes for amino acid substitutions L76P and L176P within the motor domain) harboring homologous region upstream and downstream of *KIP3* was PCR amplified from pFC51*kip3-14* [S2] and transformed into its endogenous locus in *kip3Δ::URA3* cells by selection on 5-fluoroorotic acid (5-FOA). The sequence verified mutant was crossed with *dyn1Δ* cells containing *GFP-TUB1,* and sporulated to generate *dyn1Δ kip3-14* haploid cells expressing GFP-Tubulin. Kip3 was tagged with 3YFP as previously described [S4].

To construct cells expressing a non-tagged version of Kip3 lacking the C-terminal tail domain (Kip3ΔT-LZ), *kip3ΔT-LZ* was PCR amplified from MGY1591 (Figure S6). The upstream primer annealed to the beginning of *KIP3* and the adjoining upstream region, while the downstream primer annealed to the end of the leucine zipper of *kip3ΔT-LZ* followed by a stop codon and *KIP3* 3' UTR sequence. The product was transformed by homologous recombination into the endogenous locus of *kip3Δ::URA3* cells by selection against 5-FOA. A second copy of *kip3ΔT-LZ* harboring ~500 and ~300 basepairs upstream and downstream, respectively, was amplified from this strain and co-transformed with an adjoining *KanMX* cassette linked to the second copy of *kip3ΔT-LZ*. The second copy was integrated ~400 bases downstream of the endogenous *kip3ΔT-LZ* locus, without disrupting the neighboring gene. The same strategy was used to generate 2x *KIP3*. Construction and verification of the second copy of *kip3ΔT-LZ* was designed using SnapGene software (GSL Biotech, LLC).

Cell imaging and analysis

Time-lapse movies were acquired with log phase yeast cultures grown in synthetic complete media (0.67% yeast nitrogen base without amino acids, 2% glucose, and supplemented with the appropriate amino acids) at 24°C, unless otherwise stated. Cells were mounted on 1.2% agarose pads and images acquired using a Coolsnap HQ^2 CCD camera (Photometrics, Inc.) mounted on an AxioImager M2 microscope (Carl Zeiss, Inc.) with a Piezo-electric driven Z-stage and 63X 1.4 NA Plan-APOCHROMAT oil immersion objective, driven by SlideBook software (Intelligent Imaging Innovations, Inc.).

Cells with mispositioned spindles were identified by the presence of a straight mitotic spindle that spanned the diameter of the mother cell with neither spindle pole in direct proximity to the bud neck. Cells that displayed aberrant morphologies such as grossly enlarged size, spindle breakdown, or hyper-elongated spindle within the mother were excluded from analysis. As an alternative method to generate mispositioned spindles, we attempted to utilize *kar9Δ* cells. Although elongated anaphase spindles are initially mispositioned in *kar9Δ* cells, once astral MTs enter the bud the spindles are rapidly repositioned through the Dynein pathway. This precluded the prolonged observation of bud MT dynamics in anaphase cells with mispositioned spindles. Therefore, we utilized *dyn1Δ, act5Δ, and num1Δ* cells in this study. To record the dynamic behavior of astral MTs, eight Z-section images separated by 0.75μm increments were captured every 10 s for 10 min. The three-dimensional MT length was independently determined twice for each timepoint. The parameters of MT dynamic instability were determined as previously described [S5]. To determine the growth and shortening rates in the bud, only MT plus ends within the length of the bud were scored; MTs that were curled along the bud cortex were omitted. Catastrophes were defined as transition from growth or pause into shortening. Rescues were defined as transition from shortening into growth or pause. To determine rescue

to catastrophe ratio in the mother, only MTs whose entire lifetime was encompassed within the 10 min movie were analyzed. Some bud MTs remained in the bud during the entire 10 min timelapse and thus resulted in a ratio of one. To determine MT lifetime in the mother, image stacks were captured every 6 s for a total of 10 min, whereas for bud MT lifetime image stacks were captured every 45 s for 90 min. To determine the location of rescue and catastrophe, buds were divided into three equal regions based on the size of each bud. To calculate the catastrophe frequency for each region of the bud, the number of catastrophes observed in each region was divided by the total amount of growth time in the same region. To calculate the rescue frequencies, the number of rescues observed in each region was divided by the total amount of shortening time in the same region. Time-lapse movies of *kip3-14* cells or corresponding controls were captured after 1hr incubation of log phase cultures at 37°C. During acquisition, the temperature of the sample and stage was also maintained at 37°C.

To image Kip3-3YFP and CFP-Tub1, seven Z-series images separated by 0.75μm were captured for YFP and CFP, respectively. Kip3-3YFP signal at MT plus-ends was measured with a 24 pixel spot in sum projections of Z-series images obtained using 2x2 camera binning. Kip3-3YFP localization along MTs was determined with a 4-pixel wide linescan, using the segmented line tool of ImageJ, in maximum intensity Z-series images obtained without camera binning. To determine localization of Kip3-EYFP and Kip3ΔT-LZ-EYFP, a 3-pixel wide linescan was used in 2x2 binned images. Fluorescence intensity was corrected for background fluorescence within the cell. Images in figures represent maximum fluorescence intensity Z-projections for each timepoint. Image analysis was performed using Slidebook and ImageJ (NIH) software.

Spindle Position Checkpoint assay

Cultures were grown at 24ºC to mid-log phase and then shifted to 14°C for 24 h. Cells were fixed and stained with DAPI. Cells were identified as SPOC-arrested by the presence of a

large bud and two separated nuclei within the mother compartment. Aberrant mitotic exit was scored as anucleated, multi-nucleated, or multi-budded cells.

Dynamic microtubule simulations

Simulated MT lifetimes were determined by stochastically modeling the behavior of individual MTs with a Monte Carlo technique using MATLAB (Mathworks, Inc.) code [S6]. A 10 s time interval was used to correspond with timelapse images used to measure MT lifetimes *in vivo*. MT simulations in the mother were initiated by a MT growing from 0μm length and ended when the MT depolymerized back to 0μm. Similarly, simulations of bud MTs were initiated by a MT growing from the bud neck into the bud, and ended when the MT depolymerized back to the bud neck. To model the spatial regulation of catastrophe and rescue, the transition frequencies that were determined in each third of the bud were applied stochastically to MTs within the corresponding sections of the bud. The average length of bud MTs that underwent catastrophe at the bud tip was 5μm. Therefore, the maximum length of MTs was limited to 5μm in the simulations, and catastrophe was induced when MTs exceeded this length.

Protein expression and purification

A rigor mutant of truncated, dimeric Kif5B fused to poly-lysine and a 6xHis tag (K560-G234A-polyK-6xHis) was expressed in BL21 (DE3) cells at 24°C. Protein expression was induced for 9 h using 0.1mM isopropyl β-D-1-thiogalactopyranoside (IPTG). Protein purification was performed as previously described [S7], and 20% glycerol was added to the purified kinesin before snap freezing in liquid nitrogen and storing at -80°C. Kip3 fused at the N-terminus to 6xHis (6xHis-Kip3) was expressed using baculovirus strain DR681-Kip3 and purified from insect cells as described previously [S4]. However, DTT was omitted from the lysis buffer and present at 0.5mM in the wash and elution buffers during IMAC-based purification. Following elution from

the Ni^{2+} affinity column, the sample was adjusted to 270mM NaCl. Both buffers for ion exchange chromatography were adjusted to pH 6.9. The column was developed with a linear gradient to 1M NaCl over 20 column volumes. Yeast tubulin carrying a 6xHis tag on the C-terminus of β-tubulin (Tub2-6xHis) was purified from strain MGY1 as described previously [S8], and cycled through one round of polymerization and depolymerization prior to snap freezing. Protein concentrations were calculated using the Bradford method [S9].

Microtubule dynamics assay

Flow chambers were prepared with detergent and ethanol cleaned coverslips and double-sided tape essentially as described previously [S10]. The chamber was equilibrated with BRB80 (80mM K-PIPES, 1mM EGTA, 1mM $MgCl_2$, pH 6.8) and 50μl of 1.75μg/ml K560-G234A-polyK-6xHis in BRB80 was flown into the chamber and incubated at room temperature for 5 min. The chamber was washed with 5 volumes of BRB80 and blocked for 5 min with 8mg/ml casein in 10mM Tris-HCl, pH 8.0. The chamber was then washed with 15 volumes BRB80 and subsequently blocked with 1% Pluronic-F127 and 50μg/ml casein in PBS at room temperature. After washing the chamber with 15 volumes BRB80, Alexa488-labeled, GMPCPP-stabilized double-cycled short microtubule seeds prepared from purified porcine tubulin as described [S11] were immobilized in the chamber with a 10 min incubation at room temperature. The chamber was then washed with 15 volumes of BRB80 and equilibrated with the assay buffer (80mM K-PIPES, pH 6.8, 1mM EGTA, 2mM $MgCl_2$, 50mM KCl, 1mM DTT, 0.4mg/ml casein, 1mM GTP, 1mM ATP and oxygen scavenger mix (20mM glucose, 200μg/ml glucose oxidase, 400μg/ml catalase, 0.5% β-mercaptoethanol)). Dynamic microtubules were reconstituted by flowing 1.4μM yeast tubulin, in the absence or presence of 10nM Kip3 (monomeric concentration), into the chamber. The chambers were incubated at 30°C for 15 min and then imaged at 30°C for no more than 1 h. Timelapse images were acquired using a Coolsnap HQ^2 CCD camera

(Photometrics, Inc.) mounted on an AxioImager M2 microscope (Carl Zeiss, Inc.) fitted with differential interference contrast (DIC) optics and a 100X 1.4 NA Plan-APOCHROMAT Oil DIC objective. To determine polymerization rate and catastrophe frequency images were acquired every 2 s, and to determine depolymerization rate images were acquired at 0.2 s intervals. Image sequences were flatfield corrected and background subtracted, and kymographs were constructed using ImageJ software. Polymerization and depolymerization rates were determined directly from kymographs. Catastrophe frequency was determined by dividing the total number of catastrophes observed by the total time spent polymerizing for the population of MTs. The error for *in vitro* catastrophe frequency was determined by dividing the frequency by the square root of the number of catastrophes [S12].

Supplemental References

S1. Su, X., Arellano-Santoyo, H., Portran, D., Gaillard, J., Vantard, M., Thery, M., and Pellman, D. (2013). Microtubule-sliding activity of a kinesin-8 promotes spindle assembly and spindle-length control. Nat Cell Biol *15*, 948–957.

S2. Cottingham, F. R., and Hoyt, M. A. (1997). Mitotic spindle positioning in Saccharomyces cerevisiae is accomplished by antagonistically acting microtubule motor proteins. J Cell Biol *138*, 1041–1053.

S3. Muhua, L., Adames, N. R., Murphy, M. D., Shields, C. R., and Cooper, J. A. (1998). A cytokinesis checkpoint requiring the yeast homologue of an APC-binding protein. Nature *393*, 487–491.

S4. Gupta, M. L., Carvalho, P., Roof, D. M., and Pellman, D. (2006). Plus end-specific depolymerase activity of Kip3, a kinesin-8 protein, explains its role in positioning the yeast mitotic spindle. Nat Cell Biol *8*, 913–923.

S5. Tirnauer, J. S., O'Toole, E., Berrueta, L., Bierer, B. E., and Pellman, D. (1999). Yeast Bim1p promotes the G1-specific dynamics of microtubules. J Cell Biol *145*, 993–1007.

S6. Gardner, M. K., and Odde, D. J. (2010). Stochastic simulation and graphic visualization of mitotic processes. Methods *51*, 251–256.

S7. Case, R. B., Pierce, D. W., Hom-Booher, N., Hart, C. L., and Vale, R. D. (1997). The directional preference of kinesin motors is specified by an element outside of the motor catalytic domain. Cell *90*, 959–966.

S8. Gupta, M. L., Bode, C. J., Georg, G. I., and Himes, R. H. (2003). Understanding tubulin-Taxol interactions: mutations that impart Taxol binding to yeast tubulin. Proc Natl Acad Sci USA *100*, 6394–6397.

S9. Bradford, M. M. (1976). A rapid and sensitive method for the quantitation of microgram quantities of protein utilizing the principle of protein-dye binding. Anal Biochem *72*, 248–254.

S10. Waterman-Storer, C. M. (2001). Microtubule/organelle motility assays. Curr Protoc Cell Biol *Chapter 13*, Unit 13.1.

S11. Gell, C., Bormuth, V., Brouhard, G. J., Cohen, D. N., Diez, S., Friel, C. T., Helenius, J., Nitzsche, B., Petzold, H., Ribbe, J., et al. (2010). Microtubule dynamics reconstituted in vitro and imaged by single-molecule fluorescence microscopy. Methods Cell Biol *95*, 221–245.

S12. Walker, R. A., O'Brien, E. T., Pryer, N. K., Soboeiro, M. F., Voter, W. A., Erickson, H. P., and Salmon, E. D. (1988). Dynamic instability of individual microtubules analyzed by video light microscopy: rate constants and transition frequencies. J Cell Biol *107*, 1437–1448.